Pressure-dependent reordering of valence band states in GaN/$Al_xGa_{1-x}N$ quantum wells

W. Bardyszewski
Institute of Theoretical Physics, Faculty of Physics, University of Warsaw, ulica Hoża 69, PL-00-681 Warszawa, Poland

S. P. Łepkowski
Institute of High Pressure Physics, "Unipress," Polish Academy of Sciences, ulica Sokołowska 29/37, PL-01-142 Warszawa, Poland
(Received 1 June 2011; revised manuscript received 29 September 2011; published 24 January 2012)

We show theoretically that for narrow GaN/$Al_xGa_{1-x}N$ quantum wells, lattice matched to GaN substrate and grown along the *c*-crystallographic direction a pressure-dependent reordering of the topmost valence subbands having different symmetries occurs. This reordering depends critically on the values of the D_3 and D_4 deformation potentials and can be employed in the verification of existing literature values of these parameters. In order to analyze the effect of subband reordering on the the optical properties of such systems we consider a multiband exciton problem including $\boldsymbol{k}\cdot\boldsymbol{p}$ and Coulomb coupling between subbands. Our calculations show that the difference in the exciton binding energies in different valence subbands contributes significantly to the conditions for the reordering of corresponding optical transitions in emission and absorption spectra. Pressure-induced reordering of excitonic transitions leads to a noticeable modification of the polarization of emitted/absorbed light.

DOI: 10.1103/PhysRevB.85.035318 PACS number(s): 78.55.Cr, 78.67.De, 62.50.−p

I. INTRODUCTION

Group III-N semiconductors crystallizing in the wurtzite structure have complicated valence band structures consisting of three subbands in the vicinity of the Γ point. One subband is related to the Γ_9 representation and the other two correspond to the Γ_7 representation of the symmetry group C_{6v}. Using the analogy with cubic zinc blende crystals in the framework of the so-called "regular crystal approximation" the Γ_9 level is associated with the heavy hole subband, whereas two Γ_7 subbands are termed as the light hole and the crystal-field split-off subbands.

In the unstrained bulk GaN and InN the top subband is of Γ_9 character, whereas in the bulk AlN, the sequence of subbands is inverted with the topmost Γ_7 subband. This inversion obviously is present in AlGaN alloys at high enough concentration of Al. Combining two materials such as AlGaN and GaN in one quantum well (QW) system gives an opportunity to modify the symmetry properties of the top of the valence band states. Quantum structures built with these semiconductor materials, conventionally grown along the *c*-crystallographic direction, are used to produce ultraviolet light emitters and high-power electronic devices.[1] In most cases the character of the topmost valence subband in GaN/$Al_xGa_{1-x}N$ QWs is of Γ_9 type. However, in very narrow QWs the top valence subbands are reordered with the Γ_7 subband at the top of the valence band. It was established by Shields *et al.* that this effect was responsible for the significant change of the excitonic *g* factor with the well width.[2] Proper analysis of this phenomenon requires taking into account the large biaxial strains and huge built-in electric fields (caused by piezoelectric and spontaneous polarizations) which are present in these structures and lead to dramatic modification of the electronic states of the conduction and valence bands.[1] Unfortunately, the quantitative description of this effect in the framework of the $\boldsymbol{k}\cdot\boldsymbol{p}$ method is hampered by existing discrepancies in the literature as to the exact values of relevant parameters, in particular the deformation potentials D_3 and D_4.[3]

The effect of reordering of topmost valence subbands and hence changing the emitted light polarization has been observed in nitride QWs grown along both nonpolar and semipolar (i.e., nonparallel to the *c* axis) directions.[4–6] It was shown by applying the $\boldsymbol{k}\cdot\boldsymbol{p}$ analysis that anisotropic strain in the *c* plane and shear strain are crucial in determining the ordering of the topmost valence bands (Ref. 5). Little attention has been devoted to the alternative possibility of applying external stress to change the symmetry of the topmost valence subbands. So far, hydrostatic pressure studies of the photoluminescence (PL) and absorption have been focused on the pressure dependence of interband transition energies and have been used to investigate the hydrostatic deformation potentials of the band gap in nitride bulk semiconductors and electromechanical effects in nitride QWs and quantum dots.[7–13] The role of excitons in nitride QW structures under pressure has usually been estimated using simple variational calculations.[8,14]

In the present paper, we investigate the influence of the external hydrostatic pressure on the valence band structure and excitonic optical spectra of very narrow nitride QWs grown along the *c* axis. Contrary to the previous papers which were devoted to pressure dependence of interband transition energies, we focus here on pressure-induced changes in the top of the valence band of nitride QWs. Particularly, we show that for multiple GaN/$Al_xGa_{1-x}N$ QWs with properly chosen widths of QWs and barriers, and grown on GaN substrate along the *c*-crystallographic direction, one should observe a pressure-dependent crossing between Γ_9 and Γ_7 subbands. This effect is extremely sensitive to the values of the deformation potentials D_3 and D_4. Surprisingly, the direction of the crossing (Γ_7 to Γ_9 or Γ_9 to Γ_7) with pressure and the width of the QW at which it occurs depend critically on those parameters. In order to analyze the effect of band reordering on the excitonic optical spectra we have developed an accurate multiband exciton theory which is particularly applicable for wide gap semiconductor QW structures.

Calculations performed using this model demonstrate that the excitonic effects contribute significantly to the conditions for the reordering of optical transitions.

II. MODEL

A. Single-particle states

Our studies of the pressure-induced changes in the top of the valence band are based on calculations which are performed within the framework of the continuum theory of elasticity and piezoelectricity and the $\boldsymbol{k}\cdot\boldsymbol{p}$ method using the Rashba-Sheka-Pikus valence band Hamiltonian.

The conduction band states at the zone center are described by the s-type functions $v_1 = |C,\sigma_c = \uparrow\rangle \equiv |S\rangle\uparrow$ and $v_2 = |C,\sigma_c = \downarrow\rangle \equiv |S\rangle\downarrow$, where σ_c denotes electron spin in the conduction band. Valence band basis is built of p-type functions, the eigenstates of the z projection of the orbital angular momentum with $J = 1$:

$$\begin{aligned}
u_1 &= |V,J_Z = 1,\sigma_v = \uparrow\rangle \equiv -\frac{1}{\sqrt{2}}|X + iY\rangle\uparrow,\\
u_2 &= |V,J_Z = 0,\sigma_v = \uparrow\rangle \equiv |Z\rangle\uparrow,\\
u_3 &= |V,J_Z = -1,\sigma_v = \uparrow\rangle \equiv \frac{1}{\sqrt{2}}|X - iY\rangle\uparrow,\\
u_4 &= |V,J_Z = 1,\sigma_v = \downarrow\rangle \equiv -\frac{1}{\sqrt{2}}|X + iY\rangle\downarrow,\\
u_5 &= |V,J_Z = 0,\sigma_v = \downarrow\rangle \equiv |Z\rangle\downarrow,\\
u_6 &= |V,J_Z = -1,\sigma_v = \downarrow\rangle \equiv \frac{1}{\sqrt{2}}|X - iY\rangle\downarrow.
\end{aligned} \tag{1}$$

These states are in the following labeled by a double index $J_z\sigma_v$, where $J_z = 1,0,-1$ and $\sigma_v = \uparrow,\downarrow$. In order to find energy levels in the QW system at the zone center we solve eigenequations for the envelope functions in the conduction and valence band of the general form

$$\sum_{\bar{n}} \hat{H}_{\beta,n\bar{n}}(z)F^{\beta}_{\bar{n},N}(z) = E^{\beta}_{N}F^{\beta}_{n,N}(z), \tag{2}$$

where the z axis is parallel to the growth direction. Here $\hat{H}_{\beta,n\bar{n}}(z)$ represents the Hamiltonian matrix for the conduction band ($\beta = C$) and valence band ($\beta = V$) and the summation is preformed over the indices corresponding to the basis states for the given band. The Hamiltonian matrices are taken for the vanishing momentum component perpendicular to the growth axis $\boldsymbol{p}_{\perp} = 0$, while the z component of momentum is replaced with the $-i\hbar\frac{\partial}{\partial z}$ operator. For the conduction band in the parabolic approximation we simply have a diagonal 2×2 matrix

$$\hat{H}_C = \left(-\frac{\partial}{\partial z}\frac{\hbar^2}{2m_{||}}\frac{\partial}{\partial z} + U_C(z)\right)\hat{I}_2, \tag{3}$$

where $m_{||}$ denotes z-dependent effective mass across different QW layers in the conduction band and $U_C(z)$ is the potential profile for the conduction band including band discontinuities, electric field E_z, and band renormalization due to strain. The standard symbol $\hat{I}_n$ denotes the $n\times n$ identity matrix.

The valence band Hamiltonian at $\boldsymbol{p}_{\perp} = 0$ for a given valence band potential profile $U_V(z)$ is given by a 6×6 matrix of the form

$$\begin{aligned}
\hat{H}_V = {} & U_V(z)\hat{I}_6 + \sqrt{2}\Delta_3(\hat{\sigma}_-\otimes\hat{J}_+ + \hat{\sigma}_+\otimes\hat{J}_-) + \Delta_2\hat{\sigma}_z\otimes\hat{J}_z\\
& + \hat{I}_2\otimes\left\{[\Delta_1 + D_3\varepsilon_{zz} + D_4(\varepsilon_{xx}+\varepsilon_{yy})]\hat{J}_z^2\right.\\
& \left. - \frac{\hbar^2}{2m_0}\frac{\partial}{\partial z}(A_1\hat{I}_3 + A_3\hat{J}_z^2)\frac{\partial}{\partial z}\right\}.
\end{aligned} \tag{4}$$

We have used the notation from Ref. 15: $\hat{J}_{\pm} = \frac{1}{\sqrt{2}}(\hat{J}_x \pm i\hat{J}_y)$ and $\hat{\sigma}_{\pm} = \frac{1}{2}(\hat{\sigma}_x \pm i\hat{\sigma}_y)$, where the 3×3 matrices $\hat{J}_x,\hat{J}_y,\hat{J}_z$, represent the angular momentum operator components for $J = 1$ and $\hat{\sigma}_x,\hat{\sigma}_y,\hat{\sigma}_z$ denote standard Pauli matrices. Accordingly, Δ_i, A_j are the band parameters and D_k are the deformation potentials for the valence band in wurtzite structure semiconductors. Note that the equations for the envelope functions have full symmetry with respect to the rotations about the z axis. Consequently, the eigenstates have well-defined projection of the total angular momentum on the z axis.

The potential profiles U_C and U_V contain band gap discontinuities and modifications due to strain and the built-in electric field which can be determined in the framework of the continuum theory of elasticity and piezoelectricity. Using the approach of Ref. 13, one can describe the pressure tuning of the nonzero elements of the strain tensor and the built-in electric field in GaN/Al_xGa_{1-x}N multi-QWs with unstrained QWs (i.e., grown on GaN substrate) by the following equations:

$$\varepsilon_{xx,b} = \varepsilon_{yy,b} = \frac{a_w}{a_b}\left[1 + \frac{C_{11,w} - C_{13,w}}{(C_{11,w}+C_{12,w})C_{33,w} - 2C^2_{13,w}}P\right] - 1, \tag{5}$$

$$\varepsilon_{xx,w} = \varepsilon_{yy,w} = \frac{C_{11,w} - C_{13,w}}{(C_{11,w}+C_{12,w})C_{33,w} - 2C^2_{13,w}}P, \tag{6}$$

$$\varepsilon_{zz,b} = -\frac{2C_{13,b}}{C_{33,b}}\varepsilon_{xx,b} + \frac{e_{33,b}}{C_{33,b}}E'_{z,b} + \frac{P}{C_{33,b}}(e_{33,b}E''_{z,b} - 1), \tag{7}$$

$$E_{z,b} = E'_{z,b} + PE''_{z,b}, \tag{8}$$

where

$$E'_{z,b} = \frac{L_w\left[P_{sp,w} + 2\left(e_{31,w} - \frac{C_{13,w}}{C_{33,w}}e_{33,w}\right)\varepsilon_{xx,w} - P_{sp,b} - 2\left(e_{31,b} - \frac{C_{13,b}}{C_{33,b}}e_{33,b}\right)\varepsilon_{xx,b}\right]}{L_w\kappa_b + L_b\kappa_w}, \tag{9}$$

$$E''_{z,b} = \frac{L_w}{L_w\kappa_b + L_b\kappa_w}\left(\frac{e_{33,b}}{C_{33,b}} - \frac{e_{33,w}}{C_{33,w}}\right), \tag{10}$$

$$\kappa_b = \tilde{\epsilon}_b + \frac{e^2_{33,b}}{C_{33,b}}. \tag{11}$$

In the above equations, we indicate all material tensors, fields, and parameters by indices w for the QWs and b for the barriers. Formulas for $\varepsilon_{zz,w}$, $E_{z,w}$, and κ_w can be obtained from Eqs. (7)–(11) by interchanging the indices b and w. The piezoelectric constants are denoted by e_{ij}, C_{ij} are the elastic constants, P is hydrostatic pressure, L is the width of the layer, a is the in-plane lattice constant, and $\tilde{\epsilon}$ is the electric permittivity. With the above definitions we have the following expressions for the potential profile in each layer:

$$\begin{aligned} U_C(z) &= U_{0C} + eE_z z + a_{cz}\varepsilon_{zz} + a_{ct}(\varepsilon_{xx} + \varepsilon_{yy}), \\ U_V(z) &= U_{0V} + eE_z z + D_1\varepsilon_{zz} + D_2(\varepsilon_{xx} + \varepsilon_{yy}), \end{aligned} \tag{12}$$

where the U_{0C} and U_{0V} denote the energy of the band edge in unstrained material in the conduction and the valence band, respectively. The conduction band deformation potentials are denoted by a_{cz} and a_{ct}.

Equations (2), (3) and (4) are solved by the finite element method. Note that in order to ensure the Hermiticity of operators containing the product of functions and derivatives we use the symmetrization

$$\begin{aligned} Q(z)\frac{\partial^2}{\partial z^2} &\to \frac{\partial}{\partial z}Q(z)\frac{\partial}{\partial z}, \\ Q(z)\frac{\partial}{\partial z} &\to \frac{1}{2}\left(\frac{\partial}{\partial z}Q(z) + Q(z)\frac{\partial}{\partial z}\right). \end{aligned}$$

B. Multisubband exciton theory

Due to the strong exciton effects in nitride quantum structures, it is inevitable to consider electron-hole interaction in the studies of the optical transitions. It has been pointed out that the complexity of the band structure in this case restricts the applicability of variational approaches based on the one-band electron Hamiltonians to relatively wide QWs.[16] Therefore, a multiband model of excitons in GaN/AlGaN QW at zero pressure was presented in which the hydrogen-atom-type orbitals were used as the basis for solving the exciton equation.[16] We introduce here another technique based on the expansion of the exciton wave function in the Landau orbitals corresponding to a fictitious magnetic field.[17]

In our model we solve the Bethe-Salpeter exciton equation in the minisubband $\boldsymbol{k}\cdot\boldsymbol{p}$ approximation.[18] The excitons are described using the time-dependent correlation function $\Psi_{1,2} := \Theta(t)\langle[\hat{a}_2^\dagger(t)\hat{a}_1(t), \hat{P}_\varepsilon^\dagger(0)]\rangle$, where $\hat{a}_1^\dagger$ and $\hat{a}_2$ are creation and annihilation operators for electron band states 1 and 2, respectively. The momentum operator has the form $\hat{P}_\varepsilon^\dagger(t) = \sum_{1,2} P_{1,2}^\varepsilon a_1^\dagger(t)a_2(t)$, where $P_{1,2}^\varepsilon = \langle 1|\hat{p}_\varepsilon|2\rangle$ is equal to the matrix element of $\hat{p}_\varepsilon$, the projection of the one-particle momentum operator onto the light polarization vector $\boldsymbol{\varepsilon}$. The indices 1 denote single electron states in the conduction subbands and the indices 2 denote the states in the valence subbands.

The Bethe-Salpeter equation takes the form

$$\begin{aligned} i\frac{\partial}{\partial t}\Psi_{1,2}(t) &= \sum_{\bar{1},\bar{2}}\left[\mathcal{H}_{1\bar{1}}^C\delta_{2\bar{2}} - \bar{\mathcal{H}}_{2\bar{2}}^V\delta_{1\bar{1}}\right]\Psi_{\bar{1},\bar{2}}(t) \\ &\quad - \sum_{\bar{2},\bar{1}} V_{1,\bar{2},2,\bar{1}}\Psi_{\bar{1},\bar{2}}(t) + i\delta(t)P_{1,2}^\varepsilon \\ &\equiv \sum_{\bar{1},\bar{2}}\mathcal{H}_{12,\bar{1}\bar{2}}^X\Psi_{\bar{1},\bar{2}}(t) + i\delta(t)P_{1,2}^\varepsilon. \end{aligned} \tag{13}$$

The single-particle Hamiltonian operator $\mathcal{H}_{1\bar{1}}^C$ describes the conduction band states in wurtzite QWs in the parabolic band approximation. The valence band term $\mathcal{H}_{2\bar{2}}^V$ is obtained from the Rashba-Sheka-Pikus Hamiltonian matrix for wurtzite QWs.[15] The electron-hole Coulomb interaction containing both the direct term and the exchange part is represented by $V_{1,\bar{2},2,\bar{1}}$ matrix elements. The vector $P_{1,2}^\varepsilon$ represents the initial state of the exciton after absorption of photon. In this equation the exciton Hamiltonian matrix is simply defined as

$$\mathcal{H}_{12,\bar{1}\bar{2}}^X = \left[\mathcal{H}_{1\bar{1}}^C\delta_{2\bar{2}} - \bar{\mathcal{H}}_{2\bar{2}}^V\delta_{1,\bar{1}}\right] - V_{1,\bar{2},2,\bar{1}}, \tag{14}$$

where δ_{ij} denotes the Kronecker δ and the bar over symbols denotes the complex conjugation.

Taking advantage of the axial symmetry of the problem we introduce the symmetrized basis set to describe the electron-hole pair states:

$$\begin{aligned} \Phi_{sMN\sigma_c}^{L_z}(\rho_{12}) = {\sum_{n,J_z,\sigma_v}}' &\varphi_{ns}(\rho_{12})F_{\sigma_c,M}^C(z_1)\bar{F}_{J_z\sigma_v,N}^V(z_2)|C,\sigma_c\rangle \\ &\otimes\hat{\mathcal{K}}|V,J_z\sigma_v\rangle, \end{aligned} \tag{15}$$

with L_z denoting the projection of the total angular momentum onto the z axis. A primed summation sign indicates that a restriction should be applied as discussed below. The time-reversal operator $\hat{\mathcal{K}}$ reflects the symmetry of the hole states with respect to electron states. In our approach the relative motion of the electron and hole in the QW plane represented by the two-dimensional vector $\boldsymbol{\rho}_{12} = \boldsymbol{\rho}_1 - \boldsymbol{\rho}_2 = x\boldsymbol{i} + y\boldsymbol{j}$ is described using the Landau orbitals corresponding to a fictitious magnetic field B_0 perpendicular to the QW plane. Associated with this magnetic field is the so-called magnetic length $l_0 = \sqrt{\hbar/eB_0}$, which determines the spatial extension of the Landau orbitals defined by

$$\varphi_{ns}(\rho_{12}) = \frac{(\hat{a}^\dagger)^n(\hat{b}^\dagger)^s}{l_0\sqrt{2\pi n!s!}}\exp\left(-\frac{\rho_{12}^2}{4l_0^2}\right), \tag{16}$$

where the ladder operators $\hat{a}^\dagger$ and $\hat{b}^\dagger$ are given by

$$\begin{aligned} \hat{a}^\dagger &= \frac{1}{\sqrt{2}}\left[-l_0\left(\frac{\partial}{\partial x} + i\frac{\partial}{\partial y}\right) + \frac{1}{2l_0}(x + iy)\right], \\ \hat{b}^\dagger &= \frac{1}{\sqrt{2}}\left[-l_0\left(\frac{\partial}{\partial x} - i\frac{\partial}{\partial y}\right) + \frac{1}{2l_0}(x - iy)\right]. \end{aligned} \tag{17}$$

Each Landau orbital $\varphi_{ns}(\rho_{12})$ has a well-defined z component of the angular momentum equal to $\hbar(n-s)$ so the summation in Eq. (15) is restricted by the conditions

$$L_z = n - s + \sigma_c - J_z - \sigma_v, \quad n \geqslant 0, \quad s \geqslant 0. \tag{18}$$

Operators of relative electron-hole momentum in the QW plane are expressed in terms of the ladder operators in the following way:

$$\begin{aligned} p_+ &= p_x + ip_y = \frac{i\hbar}{\sqrt{2}l_0}(\hat{a}^\dagger - \hat{b}), \\ p_- &= p_x - ip_y = \frac{-i\hbar}{\sqrt{2}l_0}(\hat{a} - \hat{b}^\dagger), \\ p_\perp^2 &= p_+p_-. \end{aligned} \tag{19}$$

The matrix elements of the conduction band part $\mathcal{H}^C_{1\bar{1}}$ of the exciton Hamiltonian in Eq. (13) in the above basis set are given by

$$\mathcal{H}^C_{M\bar{M}} = \left(\frac{p_\perp^2}{2m_\perp} + E^C_M\right)\delta_{M,\bar{M}}, \tag{20}$$

where $m_\perp$ denotes the conduction band effective mass in the direction parallel to the QW plane. The valence band part of the exciton Hamiltonian is obtained from Rashba-Sheka-Pikus Hamiltonian using six-dimensional eigenvectors $\boldsymbol{F}^V_{\bar{N}}(z)$ of Eq. (2):

$$\begin{aligned}\mathcal{H}^V_{N\bar{N}} = {} & E^V_N\delta_{N\bar{N}} + \frac{p_\perp^2}{2m_0}\int_{-\infty}^{\infty} dz\left[\boldsymbol{F}^V_N(z)\right]^\dagger\left(A_2\hat{I}_3 + A_4\hat{J}_z^2\right)\\ & \otimes\hat{I}_2\boldsymbol{F}^V_{\bar{N}}(z) - \frac{1}{2m_0}\int_{-\infty}^{\infty} dz\left[\boldsymbol{F}^V_N(z)\right]^\dagger\\ & \times A_5(p_-^2\hat{J}_+^2 + p_+^2\hat{J}_-^2)\\ & \otimes\hat{I}_2\boldsymbol{F}^V_{\bar{N}}(z) + i\frac{\hbar}{2m_0}\int_{-\infty}^{\infty} dz\left[\boldsymbol{F}^V_N(z)\right]^\dagger(p_-[\hat{J}_z,\hat{J}_+]_+\\ & + p_+[\hat{J}_z,\hat{J}_-]_+)\otimes\hat{I}_2\left(A_6\frac{\partial}{\partial z} + \frac{\partial}{\partial z}A_6\right)\boldsymbol{F}^V_{\bar{N}}(z). \end{aligned}\tag{21}$$

The Coulomb potential matrix elements in this representation are simply expressed in terms of single integrals involving the envelope functions as discussed in the Appendix.

The excitonic wave functions can be expanded in this basis in the following manner:

$$\Psi_{1,2}(t) \equiv \Psi^{L_z}(\rho_{12},t) = \sum_{sMN\sigma_c}\psi_{sMN\sigma_c}(t)\Phi^{L_z}_{sMN\sigma_c}(\rho_{12}). \tag{22}$$

The summation is carried over the subbands in the conduction band (index M), subbands in the valence band (index N), conduction electron spin σ_c and the Landau orbital index s. The projection of the total angular momentum on the z axis L_z is a good quantum number for excitons with circular polarization $\sigma_\pm$ and linear polarization σ_z with respect to the normal to QW plane. The Bethe-Salpeter equation (13) is solved by expanding the coefficients $\psi_{sMN\sigma_c}(t)$ of excitonic wave functions in the basis of the eigenstates of the Hamiltonian:[18,19]

$$H^X\Psi^\lambda = E^X_\lambda\Psi^\lambda, \tag{23}$$

where E^X_λ denotes the energy of the excitonic eigenstate Ψ^λ.

According to the linear-response theory the absorption coefficient can be written as

$$\alpha(\omega) = \frac{4\pi e^2}{cn_r m_0^2\hbar\omega L_w}\mathrm{Re}\int_0^\infty\langle[\hat{P}_\varepsilon(t),\hat{P}^+_\varepsilon(0)]\rangle e^{i(\omega+i0^+)t}dt, \tag{24}$$

where L_w is QW width, n_r is the refractive index, m_0 is electron mass, e is elementary charge, and the angular brackets represent ensemble averaging. The absorption can be expressed in terms of the exciton eigenstates Ψ^λ and takes the form

$$\alpha(\omega) = \frac{4\pi e^2}{cn_r m_0^2\hbar\omega L_w}\sum_\lambda|\langle P^\varepsilon|\Psi^\lambda\rangle|^2\delta\left(\omega - E^X_\lambda/\hbar\right). \tag{25}$$

Here we defined the product of excitonic states by

$$\langle P^\varepsilon|\Psi^\lambda\rangle = \sum_{1,2}\bar{P}^\varepsilon_{1,2}\Psi^\lambda_{1,2} = \sum_{sMN\sigma_c}\bar{P}^\varepsilon_{sMN\sigma_c}\psi^\lambda_{sMN\sigma_c}. \tag{26}$$

The initial exciton state $P^\varepsilon_{1,2}$ in the representation given in Eq. (15) is equal to

$$P^\varepsilon_{sMN\sigma_c} = \frac{\mp 1}{\sqrt{2\pi}l_0}P_{CV}\int dz\, F^C_{\sigma_c,M}(z)\bar{F}^V_{-L_z\sigma_c,N}(z), \tag{27}$$

where P_{CV} denotes the interband momentum matrix element at the bulk Brillouin zone center. The upper sign corresponds to $L_z = 1$ for circular light polarization $\varepsilon = \sigma_+$, while the lower sign corresponds to $L_z = 0$ for linear polarization $\varepsilon = \sigma_z$, and $L_z = -1$ for circular polarization $\varepsilon = \sigma_-$, respectively.

Exploiting the fact that the exciton Hamiltonian matrix in the representation of Landau orbitals is sparse, we generated the excitonic spectra using the Lanczos reduction technique using $|P^\varepsilon\rangle$ as an initial vector. The value of the fictitious magnetic field B_0 is carefully adjusted in order to increase the accuracy of calculations. This feature is particularly useful when we want to describe both a tightly bound ground state and more extended excited states and therefore it is well suited for studying excitons in wide gap semiconductors. In the present study we have taken $B_0 = 15$ T, which guarantees the accuracy of the energy of the ground state on the level of 0.05 meV and provides fairly good accuracy in describing the lower energy portion of the continuum spectrum. In order to simulate the broadening of optical spectra, we have replaced δ functions in Eq. (25) by Gaussians with the standard full width at half maximum equal to 8 meV. The emission spectra are evaluated from absorption curves using the Einstein relation and assuming the temperature of 80 K.

III. RESULTS AND DISCUSSION

A. Single-particle calculations

We analyze first the pressure dependence of the valence band structure of the GaN/$Al_xGa_{1-x}N$ QWs lattice matched to the GaN substrate. Single-particle states have been calculated using the values of the material parameters for GaN and AlN, which are listed in Table I. We employ recently calculated deformation potentials for the valence band using the density functional method with the hybrid Heyd-Scuseria-Ernzerhof functional.[3] The parameters for $Al_xGa_{1-x}N$ are estimated using the linear interpolation between binaries except for the energy gap and the spontaneous polarization, for which bowing is taken into account as in Ref. 12.

The effect on the nonlinear piezoelectricity is included assuming the strain dependence of piezoelectric constants of GaN and $Al_xGa_{1-x}N$.[22] The diagram in Fig. 1 shows the dominant [Γ_7 (stars) or Γ_9 (squares)] character of the topmost valence subband depending on the Al content in the barrier and QW width in GaN/$Al_xGa_{1-x}N$ multi-QWs system for fixed barrier thickness equal to 40 nm at pressure $P = 0$ GPa. According to Ref. 23 fully strained structures are available for this Al content range and barrier thickness. For narrow QWs, one can observe that the topmost valence subband is of Γ_7 character. With increasing the QW width, reordering of Γ_7 and Γ_9 valence band levels occurs in accordance with

TABLE I. Material parameters for GaN and AlN.

	GaN	AlN
Δ_{so} (eV)	0.017[a]	0.019[a]
Δ_{cr} (eV)	0.010[a]	−0.169[a]
m_{ez} (m_0)	0.20[b]	0.33[b]
A_1 ($\hbar^2/2m_0$)	−5.947[c]	−3.991[c]
A_2 ($\hbar^2/2m_0$)	−0.528[c]	−0.311[c]
A_3 ($\hbar^2/2m_0$)	5.414[c]	3.671[c]
A_4 ($\hbar^2/2m_0$)	−2.512[c]	−1.147[c]
A_5 ($\hbar^2/2m_0$)	−2.510[c]	−1.329[c]
A_6 ($\hbar^2/2m_0$)	−3.202[c]	−1.952[c]
$a_{cz} = a_{ct}$ (eV)	−4.6[b]	−4.5[b]
$(a_{cz} - D_1)$ (eV)	−5.81[d]	−4.31[d]
$(a_{ct} - D_2)$ (eV)	−8.92[d]	−12.11[d]
D_3 (eV)	5.47[d]	9.12[d]
D_4 (eV)	−2.98[d]	−3.79[d]
a (Å)	3.189[b]	3.112[b]
C_{11} (GPa)	366[b]	397[b]
C_{12} (GPa)	139[b]	143[b]
C_{13} (GPa)	98[b]	112[b]
C_{33} (GPa)	403[b]	372[b]
e_{31} (C/m^2)	−0.34[b]	−0.53[b]
e_{33} (C/m^2)	0.67[b]	1.5[b]
e'_{31}	−5.0[b]	−3.5[b]
e'_{33}	−16.0[b]	−15.0[b]
P_{sp} (C/m^2)	−0.034[a]	−0.09[a]
$\tilde{\epsilon}$	10.4[b]	8.5[b]
E_g (eV)	3.44[b]	6.28[b]

[a]Reference 20.
[b]Reference 12.
[c]Reference 21.
[d]Reference 3.

observations of Ref. 2. The critical well width corresponding to subband reordering, denoted as L_0, is the largest for the Al content in the barrier ranging from $x = 0.2$ to $x = 0.35$. In Figs. 2 and 3, we show analogous diagrams for pressure equal

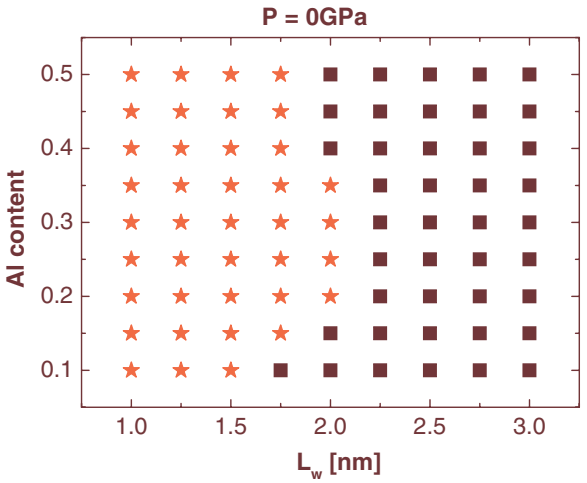

FIG. 1. (Color online) Dominant character of the uppermost valence subband in GaN/$Al_xGa_{1-x}N$ multi-QWs for various QW widths L_w and Al content in the barriers and fixed barrier width $L_b = 40$ nm. Stars correspond to the Γ_7 type of the uppermost subband and squares to the Γ_9 type.

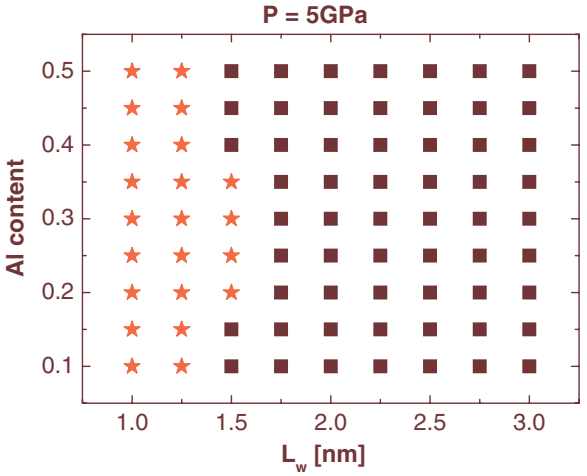

FIG. 2. (Color online) Same as in Fig. 1, but for the pressure 5 GPa.

to 5 and 10 GPa, respectively. The value of L_0 decreases with pressure for each value of the Al concentration in the barrier.

From Figs. 1–3, it is clear that for certain structures (for example GaN/$Al_xGa_{1-x}N$ QWs with $x = 0.2$, $L_w = 1.5$ nm, and barrier width $L_b = 40$ nm) it is possible to induce the Γ_7 to Γ_9 crossing by applying pressure. In order to illustrate this phenomenon we present in Fig. 4 the energy difference between the Γ_9 and Γ_7 levels, $E_{\Gamma_9} - E_{\Gamma_7}$, for such a QW (stars) as a function of pressure. The Γ_7-Γ_9 crossing is clearly seen at $P \approx 5$ GPa. We also show corresponding curves for bulk GaN (squares) and strained (lattice matched to GaN) $Al_xGa_{1-x}N$ layers for $x = 0.1$ (circles) and $x = 0.2$ (triangles). The pressure dependence of Γ_9-Γ_7 energy difference in bulk materials is significantly weaker than in the QW in which it is apparently related to the pressure-induced changes in the quantum confining potential.

Finally, we would like to note that the prediction of the pressure dependence of the Γ_9 and Γ_7 levels reordering is extremely sensitive to the values of the deformation potentials D_3 and D_4. We present in Fig. 5 the values of $E_{\Gamma_9} - E_{\Gamma_7}$ as a function of pressure for QWs with various widths obtained

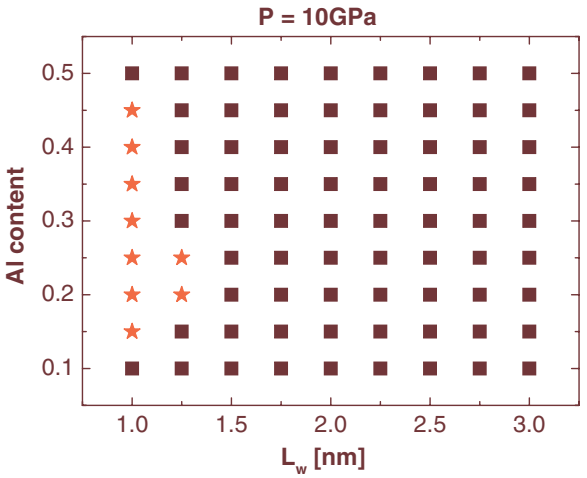

FIG. 3. (Color online) Same as in Fig. 1, but for the pressure 10 GPa.

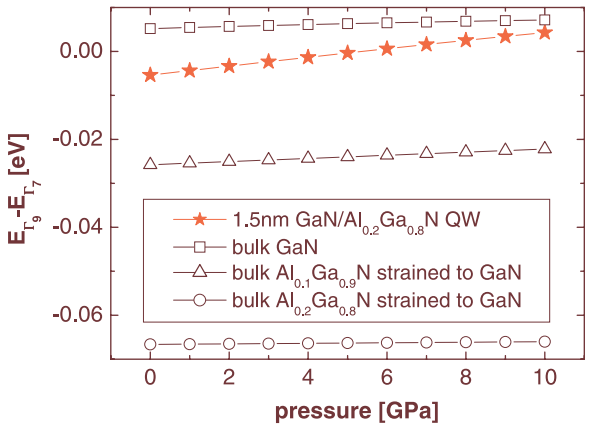

FIG. 4. (Color online) Pressure dependence of the energy difference of the two top valence levels, $E_{\Gamma_9} - E_{\Gamma_7}$ for the GaN/$Al_xGa_{1-x}N$ QW with $x = 0.2$, $L_w = 1.5$ nm, and barrier width $L_b = 40$ nm (stars), bulk GaN (squares), and strained (lattice matched to GaN) $Al_xGa_{1-x}N$ layers for $x = 0.1$ (triangles) and $x = 0.2$ (circles).

using two sets of D_3 and D_4, one from Ref. 3 (open symbols) and the other from Ref. 20 (solid symbols). One can see that using these two sets of parameters leads to opposite behavior of energy splitting with pressure. For deformation potentials from Ref. 20 we obtain the negative slope of the energy level spitting with pressure, whereas for the data from the Ref. 3 the opposite trend is observed. According to the deformation potentials determined in Ref. 3, the reordering from Γ_7 to Γ_9 levels occurs for relatively narrow QWs ($L_w = 1.5$ nm) at $p = 5$ GPa. On the other hand, for deformation potentials from Ref. 20 (solid symbols), we find that reordering from Γ_9 to Γ_7 symmetry level occurs for much wider QW $L_w = 5$ nm (triangles), while for narrow wells no reordering is possible.

B. Excitonic effects

Interband transition energies in GaN/$Al_xGa_{1-x}N$ QWs only approximately correspond to the positions of single

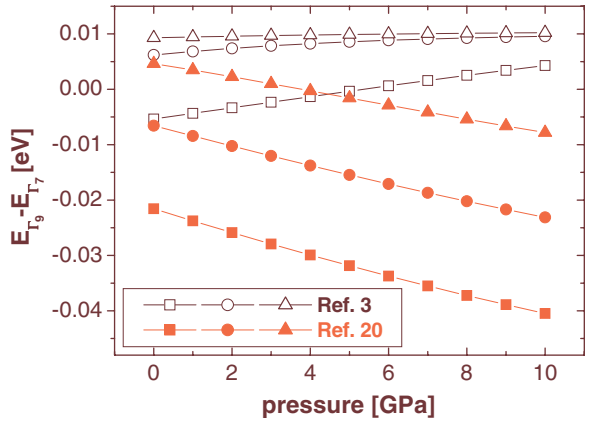

FIG. 5. (Color online) Pressure dependence of the energy difference of the two top valence levels, $E_{\Gamma_9} - E_{\Gamma_7}$ for the GaN/$Al_xGa_{1-x}N$ QW with $x = 0.2$, $L_w = 1.5$ nm (squares), $L_w = 3$ nm (circles) and $L_w = 5$ nm (triangles). Solid symbols correspond to the results obtained with deformation potentials from Ref. 20, whereas the open symbols correspond to deformation potentials from Ref. 3.

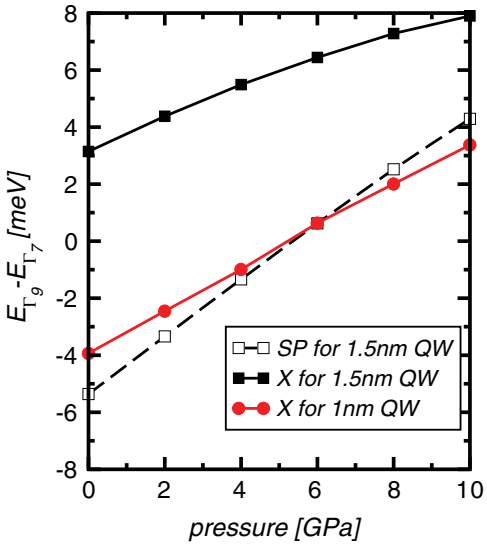

FIG. 6. (Color online) Valence band level energy difference $E_{\Gamma_9} - E_{\Gamma_7}$ (open squares) and difference of excitonic transition energies from the Γ_7 and Γ_9 to the conduction band in GaN/$Al_{0.2}Ga_{0.8}N$ QWs with $L_w = 1.5$ nm (solid squares) and with $L_w = 1$ nm (solid circles).

particle levels in the valence and conduction band due to strong excitonic effects. The difference in the exciton binding energies for Γ_7 and Γ_9 levels contributes to the conditions for the reordering of corresponding optical transitions of different symmetries.

In Fig. 6 we compare the valence band single-particle energy difference $E_{\Gamma_9} - E_{\Gamma_7}$ (open squares) with difference of excitonic transition energies from the Γ_7 and Γ_9 subbands to the conduction band (solid squares) obtained using the parameters from Table I. If not for the difference in the exciton binding energies, both curves would be identical. Since the difference in exciton binding energies is larger than Γ_9-Γ_7 level splitting, we observe that already at zero pressure the excitonic transition sequence is reversed in comparison to the single-particle picture. Increasing pressure does not lead to the reordering of excitonic transition energies, while according to the single-particle states one obtains crossing of the Γ_7 and Γ_9 levels at 5 GPa. In order to observe the reordering of excitonic transitions of different symmetry, it is necessary to use a narrower QW. Calculations including excitonic effects, performed for a QW with $L_w = 1$ nm, predict the reordering of transitions at about 5 GPa, as illustrated by the curve with full circles in Fig. 6.

Reordering of excitonic transitions is reflected in optical properties of GaN/$Al_xGa_{1-x}N$ QW structures under pressure. We show in Figs. 7 and 8 the calculated excitonic emission and absorption spectra for the 1-nm-thick GaN/$Al_{0.2}Ga_{0.8}N$ QWs at six values of pressure and two different polarizations: circular σ_+ polarization in the QW plane and linear σ_z polarization along the growth direction. Since the Γ_9 exciton transition is allowed in the σ_+ polarization and the Γ_7 exciton transition is allowed in the σ_z polarization, we observe two peaks in PL spectra, each corresponding to different polarization. The energy difference of those peaks follows the Γ_7-Γ_9 splitting depicted in Fig. 6 by the curve with full circles (note that the difference in the transition energies is equal to minus difference

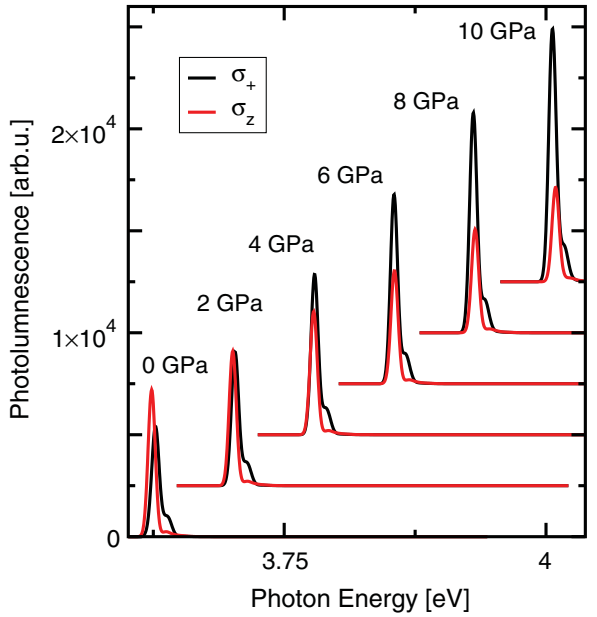

FIG. 7. (Color online) Photoluminescence evolution with pressure for circular σ_+ polarization in the QW plane (black curves) and linear, σ_z polarization parallel to the growth direction (gray curves, red online).

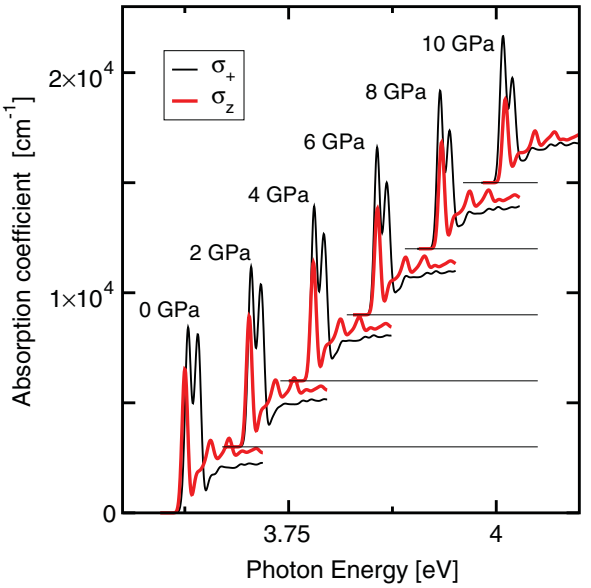

FIG. 8. (Color online) Computed absorption spectra for various pressures for circular σ_+ polarization in the QW plane (black curves) and linear σ_z polarization, parallel to the growth direction (gray curves, red online).

of the initial, valence band states). The Γ_7 emission peak intensity decreases with pressure while the Γ_9 emission peak increases. Pressure-dependent excitonic absorption spectra are illustrated in Fig. 8, in which the absorption curves for two polarizations (gray curves, red online, for σ_z and black curves for σ_+) at different pressures are presented. The excitonic transition with σ_z polarization (associated with Γ_7 levels) has lower energy than the transition at σ_+ (from Γ_9 levels) at zero pressure. The reordering of the fundamental transition peaks occurs at about $P = 5$ GPa.

IV. CONCLUSIONS

We have investigated the influence of external hydrostatic pressure on the electronic structure of the valence band in GaN/$Al_xGa_{1-x}N$ QWs. We have found that for structures with properly chosen widths of the QWs and barriers and lattice matched to GaN substrate, the pressure-dependent reordering of Γ_9-Γ_7 valence subbands occurs. This reordering depends crucially on the values of the deformation potentials D_3 and D_4. It may even have opposite behavior as a function of pressure for two examined sets of values given in Refs. 3 and 20. In order to analyze the effect of subband reordering on the the optical properties of such systems we have solved a multiband exciton problem including $\boldsymbol{k}\cdot\boldsymbol{p}$ and Coulomb coupling between subbands. Our calculations have revealed that the difference in the exciton binding energies for Γ_7 and Γ_9 levels contributes significantly to the conditions for the reordering of corresponding optical transitions in emission and absorption spectra. Change of symmetry of the dominant excitonic transition is reflected in the pressure dependence of the polarization of the emitted/absorbed light. We believe that our results will inspire high-pressure experiments on light polarization switching in semiconductor quantum structures. In particular, such studies could help in verifying the values of the deformation potentials D_3 and D_4.

ACKNOWLEDGMENTS

This work was supported by the Polish State Committee for Scientific Research, Project No. NN202 010134.

APPENDIX

In this appendix we describe our method of calculating Coulomb interaction matrix elements in the Landau basis representation. We have assumed that the dielectric permittivity $\tilde{\epsilon}$ responsible for screening is isotropic and uniform across the QW and barrier region. Although the anisotropy of the permittivity constant can be easily incorporated by a proper transformation of variables, its effect is very small in GaN.[17] Similarly, the assumed uniformity of the dielectric permittivity is well justified since the difference between $\tilde{\epsilon}$ in GaN QW and AlGaN barrier is not higher than 15%.

The direct Coulomb interaction matrix elements in the representation $\Phi^{L_z}_{sMN\sigma_c}(\rho_{12})$ defined in Eq. (15) can be easily reduced to a single integral,

$$\left\langle \Phi^{L_z}_{sMN\sigma_c}\left|\frac{1}{r_{12}}\right|\Phi^{L_z}_{s'M'N'\sigma_c}\right\rangle = \int_{-\infty}^{\infty}\frac{dk_z}{2\pi}\mathcal{M}^{C}_{\sigma_c MM'}(k_z)\bar{\mathcal{M}}^{V}_{NN'}(k_z) \times \langle\varphi_{ns}|V_{k_z}(\rho_{12})|\varphi_{n's'}\rangle, \quad \text{(A1)}$$

where the "form factors" for the conduction and valence band states are defined by

$$\mathcal{M}^{C}_{\sigma_c MM'}(k_z) = \int_{-\infty}^{\infty} dz\, e^{-ik_z z}\bar{F}^{C}_{\sigma_c M}(z)F^{C}_{\sigma_c M'}(z) \quad \text{(A2)}$$

and

$$\mathcal{M}^{V}_{NN'}(k_z) = \sum_{J_z\sigma_v}\int_{-\infty}^{\infty} dz\, e^{-ik_z z}\bar{F}^{V}_{J_z\sigma_v,N}(z)F^{V}_{J_z\sigma_v,N'}(z), \quad \text{(A3)}$$

respectively. We have also introduced

$$V_{k_z}(\rho_{12}) = \int \frac{d^2q}{(2\pi)^2} \frac{4\pi e^{i\mathbf{q}\cdot\boldsymbol{\rho}_{12}}}{q^2 + k_z^2}. \tag{A4}$$

Following the derivation in Ref. 17 for $p = n - n' \geqslant 0$ one obtains

$$\langle \varphi_{ns} | V_{k_z} | \varphi_{n's'} \rangle = (-1)^{s+s'} \sqrt{\frac{n!s'!}{n'!s!}} n'! L_{s'}^{p}(-X_0) \times U(n'+1, 1-p, X_0), \tag{A5}$$

where $X_0 = l_0^2 k_z^2/2$, $U(a,b,z)$ is the confluent hypergeometric function and $L_{s'}^{p}(X)$ denotes the Laguerre polynomial.[24]

The exchange term is given by

$$\left\langle \Phi^{L_z}_{sMN\sigma_c} \middle| V^X \middle| \Phi^{L_z}_{s'M'N'\sigma_c'} \right\rangle = -\frac{J_T}{2\pi l_0} \int dz\, F^{V}_{J_z\sigma_c,N}(z) \bar{F}^{V}_{J_z'\sigma_c',N'}(z) \times \bar{F}^{C}_{\sigma_c M}(z) F^{C}_{\sigma_c' M'}(z), \tag{A6}$$

where $J_z = \sigma_c - L_z$ and $J_z' = \sigma_c' - L_z'$. The exchange constant J_T is determined to reproduce the singlet-triplet splitting in bulk GaN, as estimated in Ref. 25.

[1] H. Morkoc, *Nitride Semiconductors and Devices* (Springer-Verlag, Berlin, Heidelberg, New York, 1999).

[2] P. A. Shields, R. J. Nicholas, N. Grandjean, and J. Massies, Phys. Rev. B **63**, 245319 (2001).

[3] Q. Yan, P. Rinke, M. Scheffler, and C. de Walle, Appl. Phys. Lett. **95**, 121111 (2009).

[4] M. Ueda, M. Funato, K. Kojima, Y. Kawakami, Y. Narukawa, and T. Mukai, Phys. Rev. B **78**, 233303 (2008).

[5] Q. Yan, P. Rinke, M. Scheffler, and C. V. de Walle, Appl. Phys. Lett. **97**, 181102 (2010).

[6] C.-N. Chen, S.-H. Chang, M.-L. Hung, J.-C. Chiang, I. Lo, W.-T. Wang, M.-H. Gau, H.-F. Kao, and M.-E. Lee, J. Appl. Phys. **102**, 043104 (2007).

[7] G. Vaschenko, D. Patel, C. S. Menoni, S. Keller, U. K. Mischra, and S. P. Baars, Appl. Phys. Lett. **78**, 640 (2001).

[8] G. Vaschenko, D. Patel, C. Menoni, H. Ng, and A. Cho, Appl. Phys. Lett. **80**, 4211 (2002).

[9] P. Perlin, I. Gorczyca, T. Suski, P. Wisniewski, S. Lepkowski, N. Christensen, A. Svane, M. Hansen, S. DenBaars, B. Damilano *et al.*, Phys. Rev. B **64**, 115319 (2001).

[10] H. Teisseyre, T. Suski, S. P. Lepkowski, P. Perlin, G. Jurczak, P. Dluzewski, B. Daudin, and N. Grandjean, Appl. Phys. Lett. **89**, 051902 (2006).

[11] H. Teisseyre, A. Kaminska, G. Franssen, A. Dussaigne, N. Grandjean, I. Grzegory, B. Lucznik, and T. Suski, J. Appl. Phys. **105**, 063104 (2009).

[12] S. P. Lepkowski, J. A. Majewski, and G. Jurczak, Phys. Rev. B **72**, 245201 (2005).

[13] S. P. Lepkowski and J. A. Majewski, Phys. Rev. B **74**, 035336 (2006).

[14] S. Ha and S. Ban, J. Phys. Condens. Matter **20**, 085218 (2008).

[15] S. L. Chuang and C. S. Chang, Phys. Rev. B **54**, 2491 (1996).

[16] E. P. Pokatilov, D. L. Nika, V. M. Fomin, and J. T. Devreese, Phys. Rev. B **77**, 125328 (2008).

[17] M. Sobol and W. Bardyszewski, Phys. Rev. B **73**, 075208 (2006).

[18] W. Bardyszewski and D. Yevick, Phys. Rev. B **49**, 5368 (1994).

[19] W. Bardyszewski, D. Yevick, Y. Liu, C. Rolland, and S. Bradshaw, J. Appl. Phys. **80**, 1136 (1996).

[20] I. Vurgaftman and J. R. Meyer, J. Appl. Phys. **94**, 3675 (2003).

[21] P. Rinke, M. Winkelnkemper, A. Qteish, D. Bimberg, J. Neugebauer, and M. Scheffler, Phys. Rev. B **77**, 075202 (2008).

[22] K. Shimada, T. Sota, K. Suzuki, and H. Okumura, Jpn. J. Appl. Phys. **37**, L1421 (1998).

[23] D. Holec, Y. Zhang, D. S. Rao, M. Kappers, C. McAleese, and C. Humphreys, J. Appl. Phys. **104**, 123514 (2008).

[24] M. Abramowitz and I. Stegun (editors), *Handbook of Mathematical Functions with Formulas, Graphs, and Mathematical Tables* (National Bureau of Standards, Gaithersburg, MD, 1972).

[25] R. Stepniewski, M. Potemski, A. Wysmolek, K. Pakula, J. M. Baranowski, J. Lusakowski, I. Grzegory, S. Porowski, G. Martinez, and P. Wyder, Phys. Rev. B **60**, 4438 (1999).